Med Bio Eng Comput (2007) 45:661–669
DOI 10.1007/s11517-007-0205-y

ORIGINAL ARTICLE

A novel simulation algorithm for soft tissue compression

Christos Zyganitidis · Kristina Bliznakova · Nicolas Pallikarakis

Received: 24 October 2006 / Accepted: 11 May 2007 / Published online: 6 June 2007

Abstract This paper presents a novel general approach to simulation of soft tissue compression. A theoretical framework of the compression algorithm has been developed and implemented, based on the concept of a simple spring. The volume subjected to compression is divided into a number of ''model elements'', each one consisting of 27 nodes. The nodes are connected with springs. The mechanical properties of the tissues are assumed to be linear and isotropic. The compressed volume remains constant due to the introduced concept of spring variable equilibrium lengths. Initial settings for compression simulation are introduced in order that the algorithm converges faster. The developed compression algorithm was used to model breast compression during a standard mammography examination. Specifically, the method was applied to a high-resolution three-dimensional software breast phantom, composed to have a medium glandularity and calcification abnormalities. The compression was set to 50%. Results showed that the abnormalities maintain their shape and dimensions during the compression, while the surrounding breast tissues undergo considerable deformation and displacement. A ''decompression'' algorithm was also applied to test the reversibility of the model.

Keywords Soft tissue compression modeling · Breast compression · Abnormalities deformation

C. Zyganitidis · K. Bliznakova · N. Pallikarakis (✉)
Department of Medical Physics, School of Medicine, University of Patras, 26500 Rio, Patras, Greece
e-mail: nipa@upatras.gr
URL: http://bme.med.upatras.gr/bit

1 Introduction

While deformable models have been extensively used in a large number of fields in the past, their applications in simulating soft tissue deformations was only recently implemented. Deformable volumes can be presented with mass-spring models [8], B-splines [12], implicit surfaces [7] and finite element models (FEM). Although these techniques are quite successful in most cases, they lack the ability to simulate the compression of a high-resolution volume within a reasonable time frame and to generate accurate results [4, 9]. Additionally, they are characterized by difficulties in their implementation, considerable computing time [1] and requirement of significant mathematical knowledge. Among these methods, only FEM were used to model breast compression. The deformation of a human female breast was modeled using data reconstructed from MRI images [2, 3]. The properties of the virtual deformable breast model were based on the use of finite elements with nonlinear material properties.

Breast compression is an essential part of mammography and is an important component in producing high quality mammographic images. Breast compression optimizes the image quality and hence the visualization of small lesions by reducing the breast thickness [10]. A proper compression also reduces the radiation dose to the breast, since the X-rays pass through shortened breast thickness and therefore their attenuation decreases as well. Finally, the compression minimizes the patient's breast movement, which would eventually cause blurring effects in the mammograms.

Breast compression is a physical process relevant to the processes of tissue shiftiness and deformations. During mammographic examination, X-rays pass through the

compressed breast, reach the detector and provide the mammographic projection image. In case abnormalities are present, their positions in the obtained mammogram are actually the corresponding positions in the compressed breast. This situation introduces some difficulties in cases where samples must be taken from the malignant area in order to perform a biopsy of the uncompressed breast [1]. Computer simulation could contribute in solving such difficulties by revealing the degree of deformation of the abnormality and their displacement, compared to the deformation of the whole breast tissue. Additionally, it would allow comparative studies of breast imaging techniques with or without the compression process.

The objective of this work was to develop a new general algorithm for simulating soft tissue compression and to apply it in the case of breast compression during a standard X-ray mammography examination. Previously, we reported a 3D breast software phantom that could be used in mammographic studies [5, 6]. In order to perform a real mammographic simulation, a compression of this 3D breast model had to be developed and implemented. This reveals possibilities to study different breast imaging techniques involving compressed and uncompressed breasts. This novel approach is based on the concept of a simple spring applied on any soft tissue volume. There are a number of novelties introduced in the simulation algorithm for soft tissue compression (SASTC). Among them is that compression solution is reached using random processes based on simple rules and boundary restrictions. The user interaction is necessary only to set the boundary conditions, while the convergence is always achieved following an exponential curve regardless of the structure and complexity of the volume under compression. Additionally, this method is suitable to handle a high-resolution volume within a reasonable time frame. The SASTC has been tested using a 3D software breast phantom with dimensions of $512 \times 512 \times 512$ mm^3 in order to study the breast deformations that occur during mammography. Breast decompression was also simulated.

2 Methods

2.1 The compression model

2.1.1 Basic model components

For the purposes of the compression model, the following terms are introduced: (a) model; (b) elements; (c) nodes; and (d) springs between the nodes. The *model* is the volume of interest subjected to compression simulation. This volume is divided into *elements* that are composed of a set of N•M•K voxels. For the sake of clarity, we introduced the term *node* to represent the voxel. Each node is surrounded by other nodes. The cube, shown in Fig. 1a, introduces the definition of the model element. Elements consist of 27 nodes, as each one (except the boundary nodes) is connected with 26 neighbor nodes. Each element has a corresponding node at its center; thus the elements are as many as the nodes and the center of each element overlaps with its central node.

The nodes in the elements are connected with *springs*. A simple spring can be defined by two parameters: modulus of elasticity E and equilibrium length, D_{eq} (Fig. 1b). Suppose that a spring is deformed to a new length D. This action will result in a force F that will appear at the spring edges, in a direction parallel to the spring and of magnitude given by Eq 1,

$$F = \frac{(D_{eq} - D)}{D_{eq}} \cdot E \tag{1}$$

For the sake of simplicity, in this work, the spring modulus of elasticity is assumed to be linear and isotropic. This means that E has a constant value for all the range of deformations that can be applied on the spring.

Each node represents a tissue sample and hence it inherits the modulus of elasticity of that tissue. The spring between a central and one of its surrounding nodes in an element has three components in the x, y and z directions. To simplify the model, the value of the modulus of elasticity between two springs is assumed to be equal to the

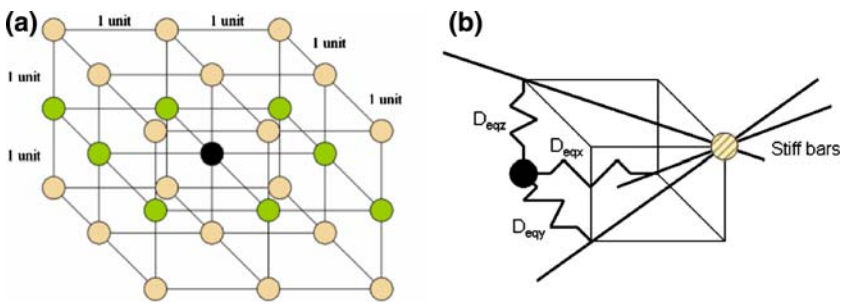

Fig. 1 Model components: **a** element of the model, **b** equilibrium lengths of the springs between a central and one of its surrounding nodes

smaller one. An important aspect here is that the calculation of the spring modulus of elasticity between every two nodes has to be the same, regardless of which one of the two nodes is the central node.

2.1.2 Element compression and volume preservation

Each *element* is divided into eight *sub-elements*. A *sub-element* is composed of eight nodes, some of which are common with other sub-elements (Fig. 2). The mean compression of a sub-element can be easily calculated as follows:

$$\Delta z_{\text{mean}} = \frac{(N_{001} - N_{000}) + (N_{101} - N_{100}) + (N_{011} - N_{010}) + (N_{111} - N_{110})}{4} \tag{2}$$

In order to keep the volume under compression constant, the concept of spring *variable equilibrium lengths* that depend on the compression level is introduced. For this purpose, the spring equilibrium lengths $D_{\text{eq}x}$ and $D_{\text{eq}y}$ are recalculated according to Eq 3. The variable N_{xyz}, shown in Fig. 2 and Eq. 2, represents the z position of the node in the volume under compression. The new x and y dimensions of the sub-element are defined by means of expression 3, assuming that the expansion along the axis x is equal to the expansion along the axis y.

$$\begin{matrix} \Delta z \cdot \Delta y \cdot \Delta x = 1 \\ \Delta y = \Delta x \end{matrix} \quad \Delta x = \Delta y = \sqrt{\frac{1}{\Delta z}} \tag{3}$$

where Δx, Δy and Δz represent the x, y and z dimensions of the sub-element. The tissues that correspond to the sub-elements can be considered homogeneous and therefore the sub-elements can expand symmetrically in the xy plane during its compression. An important point here is that the equilibrium lengths (the dimensions) that are calculated between any two nodes should be the same, regardless of which of the two nodes is considered to be the central node.

2.1.3 Equilibrium conditions

The forces that arise between a central and its surrounding nodes are graphically depicted in Fig. 3. According to the law of action–reaction, the forces that act on a central node when it is driven out of its equilibrium are equal in magnitude, and with an opposite sign, to the forces that act on its surrounding nodes.

In order that the central node is in equilibrium with its neighbors, it is moved to a new position. This position can be defined as follows:

$$\begin{aligned} X_{\text{equilibrium}} &= \frac{F_{1x} + F_{2x} + \cdots + F_{26x} + Fx_{\text{external}}}{E_{1x} + E_{2x} + \cdots + E_{26x}} + X\text{o} \\ Y_{\text{equilibrium}} &= \frac{F_{1y} + F_{2y} + \cdots + F_{26y} + Fy_{\text{external}}}{E_{1y} + E_{2y} + \cdots + E_{26y}} + Y\text{o} \\ Z_{\text{equilibrium}} &= \frac{F_{1z} + F_{2z} + \cdots + F_{26z} + Fz_{\text{external}}}{E_{1z} + E_{2z} + \cdots + E_{26z}} + Z\text{o} \end{aligned} \tag{4}$$

where F_{ix}, F_{iy}, F_{iz} are the forces along x, y and z axis that are exerted on the central node due to its surrounding nodes, and Fx_{external}, Fy_{external}, Fz_{external} are the corresponding forces that are exerted on the central node due to external factors (i.e. gravity). If the central node is translated from a point (X_{o}, Y_{o}, Z_{o}) to a point ($X_{\text{equilibrium}}$, $Y_{\text{equilibrium}}$, $Z_{\text{equilibrium}}$), the net forces that will act on it at this new position, according to expression 4, will be zero

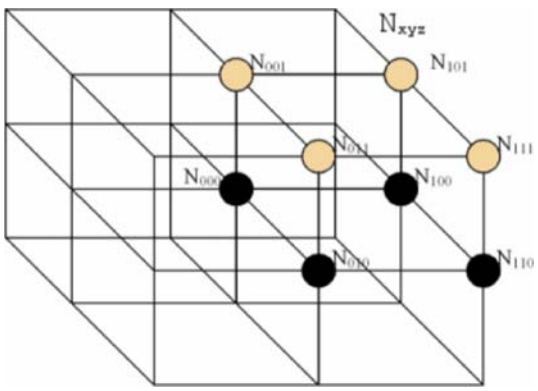

Fig. 2 The sub-element of an element

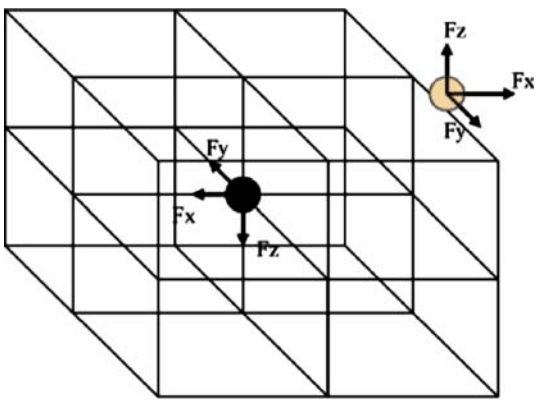

Fig. 3 Forces between a central and one of the surrounding nodes

and the central node will be in equilibrium relative to its neighbors.

2.2 Implementation

2.2.1 Initial settings

In order that the algorithm converges faster, proper initial settings that approximate the final state as closely as possible should be defined. A simple method is to compress the volume, assuming the latter to be homogenous. This however could lead to initial conditions that could be quite far from the real, leading to increased number of iterations and long computation time. For the purposes of this work, the initial conditions are set using the simple rule of action–reaction and the Hooke's law. More specifically, when n linear springs (Fig. 4) are connected in series, the force of spring 1 is transmitted to spring 2 and so on. Following this dependence, the distribution of the compression on each spring is easily calculated if the total compression of the n springs in series (Δl_{total}) is known. If this simple rule is applied to the volume, the final position of each element could be predicted before the implementation of the basic algorithm and therefore faster convergence can be achieved.

2.2.2 Method outline

The main steps in the proposed SASTC are summarized in Fig. 5. The simulation program, implemented in Java, starts by applying the initial settings to the soft tissue volume in order that the algorithm converges faster. At each iteration, an element is selected randomly and its central node is translated to a position where it is in equilibrium relative to its 26 neighbors. All model elements are processed per iteration. The convergence is monitored by calculating the net forces exerted before their equilibrium on all the nodes. This way, the average movement of the nodes is calculated. If the latter is within a given accuracy (ε), the computation is interrupted. If not, the algorithm continues with a new iteration. The convergence algorithm always is accomplished within a limited number of iterations.

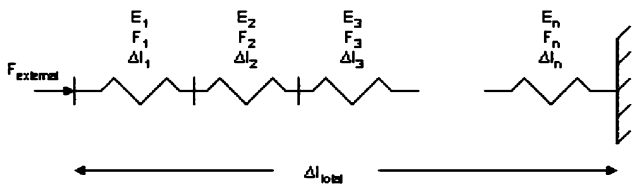

Fig. 4 Linear springs connected in series

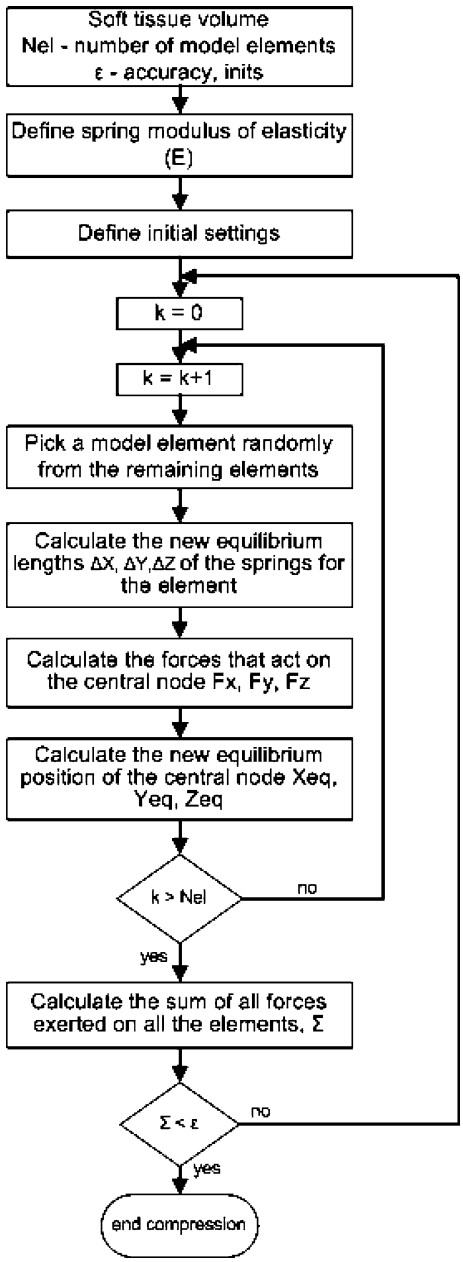

Fig. 5 Schematic diagram of the compression algorithm

2.3 The 3D breast application

The proposed SASTC was applied to study the level of deformation and displacement of the breast tissue using a 3D software breast phantom [5]. For this purpose, a 3D breast phantom composed of 50% glandular and 50% fatty tissue was composed as shown in Fig. 6. In additional to the normal breast content, calcifications with size ranging from 1.2 to 2 cm were simulated. In this figure, the gland tissue is the tree-like structure, the ellipsoids represent a number of abnormalities and the rest of the breast is filled with fat. The final breast model

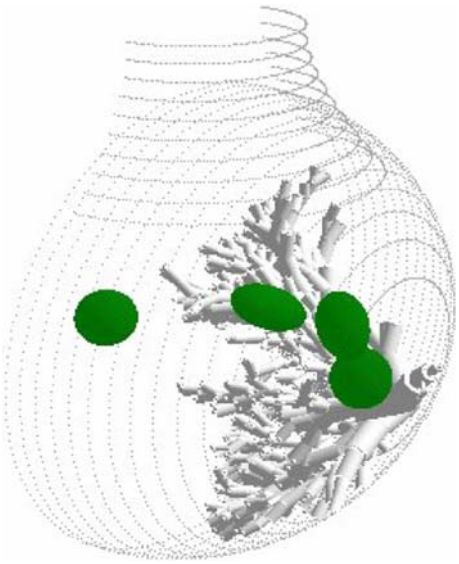

Fig. 6 A 3D breast phantom showing the duct tree system and four calcifications with sizes smaller than 2 cm

represented a 3D volume used in the compression simulation.

3 Results

Qualitative and quantitative approaches were used to evaluate the proposed algorithm for compression using the breast phantom. Qualitatively, the results of the compression algorithm were given as a series of graphical representations of the compressed breast phantom. Quantitatively, convergence curves and accuracy calculations were assessed. A deviation estimator was introduced to model the average deviation of the elements' nodes during the compression algorithm. Additionally, a reverse simulation (decompression) of the compressed breast phantom was performed in order to verify the validity of both, the compression algorithm and the proposed deviation estimator.

The generated 3D breast volume consisted of numerical values that uniquely specify the human breast tissues. For each tissue, the *modulus of elasticity* is defined according to published data by Wellman et al. [11]:

$$E_{\text{fat}} = 4.5\,\text{k}\,\text{Nm}^{-2}, \quad E_{\text{gland}} = 15\,\text{k}\,\text{Nm}^{-2},$$
$$E_{\text{abnormality}} = 45\,\text{k}\,\text{Nm}^{-2}.$$

The abnormal tissue corresponded to a calcification, modeled as $CaCO_3$. The modeled compression procedure using two compression paddles is shown in Fig. 7a. The upper paddle is placed at a height that corresponds to 85 units, while the lower paddle is set at 35 units; therefore, a 50% compression was simulated. Each unit represented 1.5 mm. For comparison, Fig. 7b shows the 3D breast model in its uncompressed form.

The *boundary conditions* in the case of breast compression during mammography are the chest region that restrains the tissue movement in any direction, and the compression paddles that restrict the movement of the tissue only in z direction.

3.1 Subjective evaluation

Figure 8a–f compares slices with thickness of 2 mm taken laterally, frontally and craniocaudally extracted from the uncompressed and the compressed breast models.

A detailed analysis is presented in Fig. 9a–h, where visual and numerical information for the value of deformation and shiftiness could be obtained. Figure 9a shows a slice taken laterally from the breast volume in a normal state. As a result of the applied compression (Fig. 9b), the breast edges expanded in the zx plane by 6 units that corresponded to 9 mm. The breast abnormalities were also displaced by more than 5 units, which in the current example was 7.5 mm. The same results are

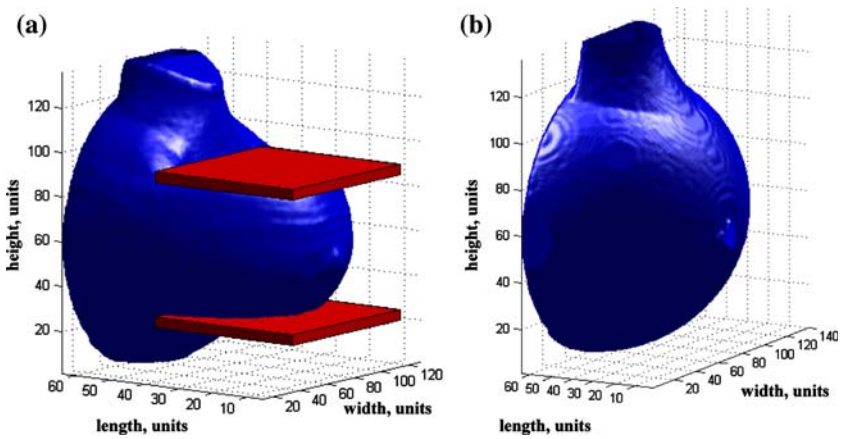

Fig. 7 Breast phantom in (**a**) a compressed and (**b**) an uncompressed aspect

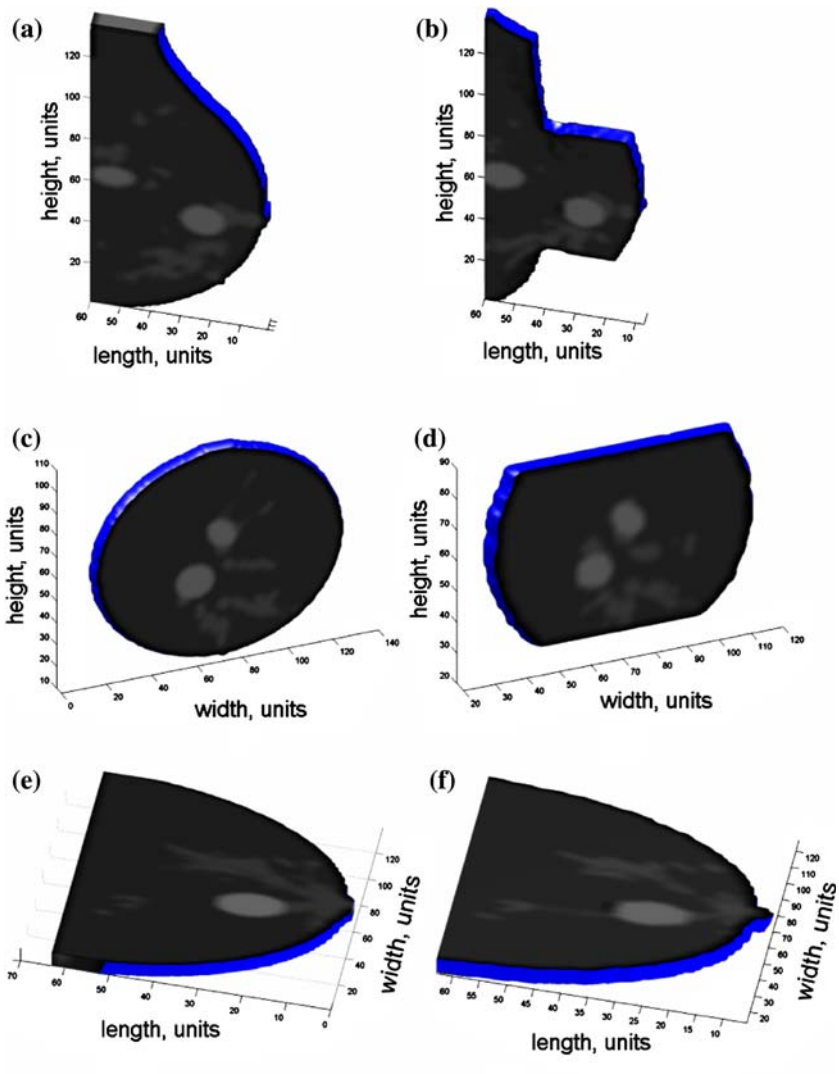

Fig. 8 Breast slices taken laterally (**a**, **b**); frontally (**c**, **d**) and craniocaudally (**e**, **f**). The slices, shown in the *left column* are taken from the uncompressed breast model, while those in the *right column* correspond to slices taken from the compressed breast model

obtained by the comparison of Fig. 9c with 9d. Figure 9e–h depicts the comparison between uncompressed and compressed breast slices, and more specifically the expansion process along the breast width during the compression process.

3.2 Convergence curve and accuracy

The convergence curves obtained along x, y and z-axes from the demonstrated simulation are presented in Fig. 10. The vertical axis represents the sum of the absolute values of the displacements of all model elements as a function of the iteration number. The average deviation is calculated as a sum of all movements of each point for all iterations, which would follow if the simulation continued infinitely. The simulation terminates when the average displacement of the nodes in the 3D object drops under a threshold value, ε. The latter was set to 10^{-4} units. This condition was found to be a good time–accuracy balance. Furthermore, the calculated average displacement was exponentially fit using Eqs. 5 and 6.

$$y_{\text{average}} = \exp(-a \times x + b) \tag{5}$$

$$\text{Deviation} = \sum_{x} y_{\text{average}}(x) = \int_{\text{total\_iterations}}^{+00} y_{\text{average}}\,\mathrm{d}x = \int_{\text{total\_iterations}}^{+00} \exp(-a \times x + b)\,\mathrm{d}x \tag{6}$$

According to these expressions, the average deviation was found to be equal to 0.062 units.

3.3 Reverse simulation

The deviation estimator and the compression algorithm were assessed by means of a reverse simulation. The

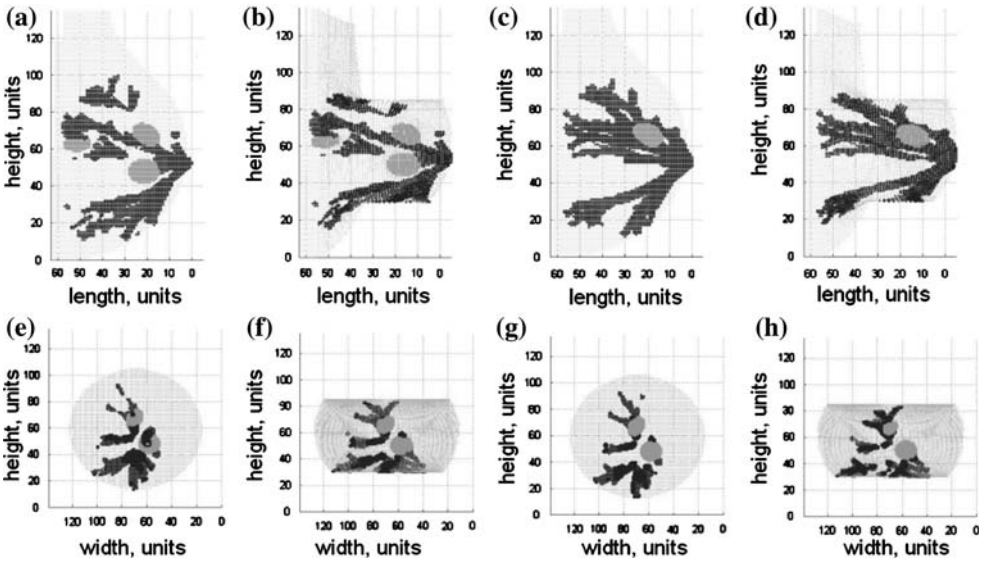

Fig. 9 Breast slices taken laterally (**a**–**d**) and frontally (**e**–**h**). The slices in (**a**), (**c**), (**e**), (**g**) are taken from the uncompressed breast model, while those in (**b**), (**d**), (**f**) and (**h**) correspond to slices taken from the compressed breast model

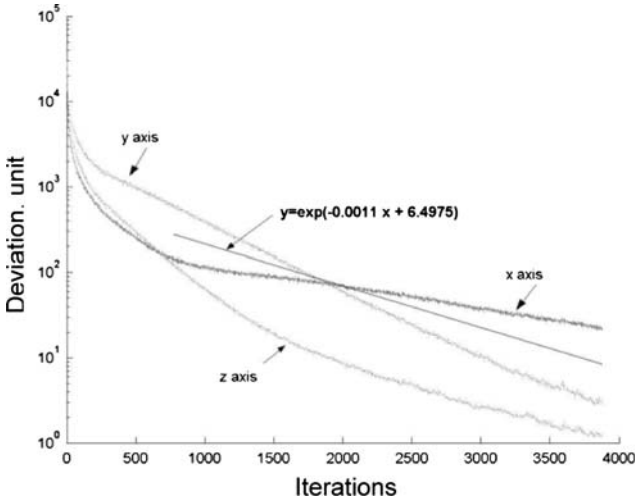

Fig. 10 Convergence curves for the demonstrated simulation

compressed breast phantom was subjected to a decompression algorithm starting by removing the compression paddles. The results of the reverse simulation are presented in Fig. 11a–e as a function of the iteration number.

The visual inspection of these figures showed that the breast phantom regained its initial shape and geometry with slight variations. The decompression process demonstrated also that the thickness of the breast was rapidly regained, but the length dimension reached its initial state slowly. In order to obtain the desired accuracy of 10^{-4} units, a total of 4,300 iterations were performed.

During the reverse simulation, the true deviation is calculated by subtracting the current node position from its position in the initial uncompressed condition. The results are shown in Fig. 12, where the calculated and estimated deviations are compared. These results demonstrate that this estimator can indeed predict a node deviation from its final equilibrium with an error that does not exceed 2% of the unit, which corresponds to 0.03 mm.

3.4 Implementation results

The breast model used for the compression simulation consisted of 512^3 nodes. All these nodes were processed in less than 12 h using a PC with AMD Athlon 2400+, 512 Mb RAM configuration.

4 Discussion

The proposed SASTC is a general algorithm and can be applied to any volume, regardless of its dimensions. The latter are limited only by the available computer configuration. This method, as seen from the flow chart in Fig. 5, is characterized by its simplicity and ease of implementation. It can be performed in any programming language by users who posses little programming knowledge. The only specificity is definition of the initial setups that aim at a faster algorithm execution. These settings depend on the simulated case. In additional to its simplicity, the method is characterized by an acceptable computational speed. The process of randomly choosing a model element, which should be subjected to compression, is an approach that also contributes to accelerated computational time. This computation time is expected to decrease with the implementation of the method on the distributed grid computer system, available in the laboratory (http://www.bme.med.upatras.gr/bit/). Moreover, the user interaction is minimized by dismissing the tedious and time-consuming need for a mesh generation and using a fully automated voxel-based model instead.

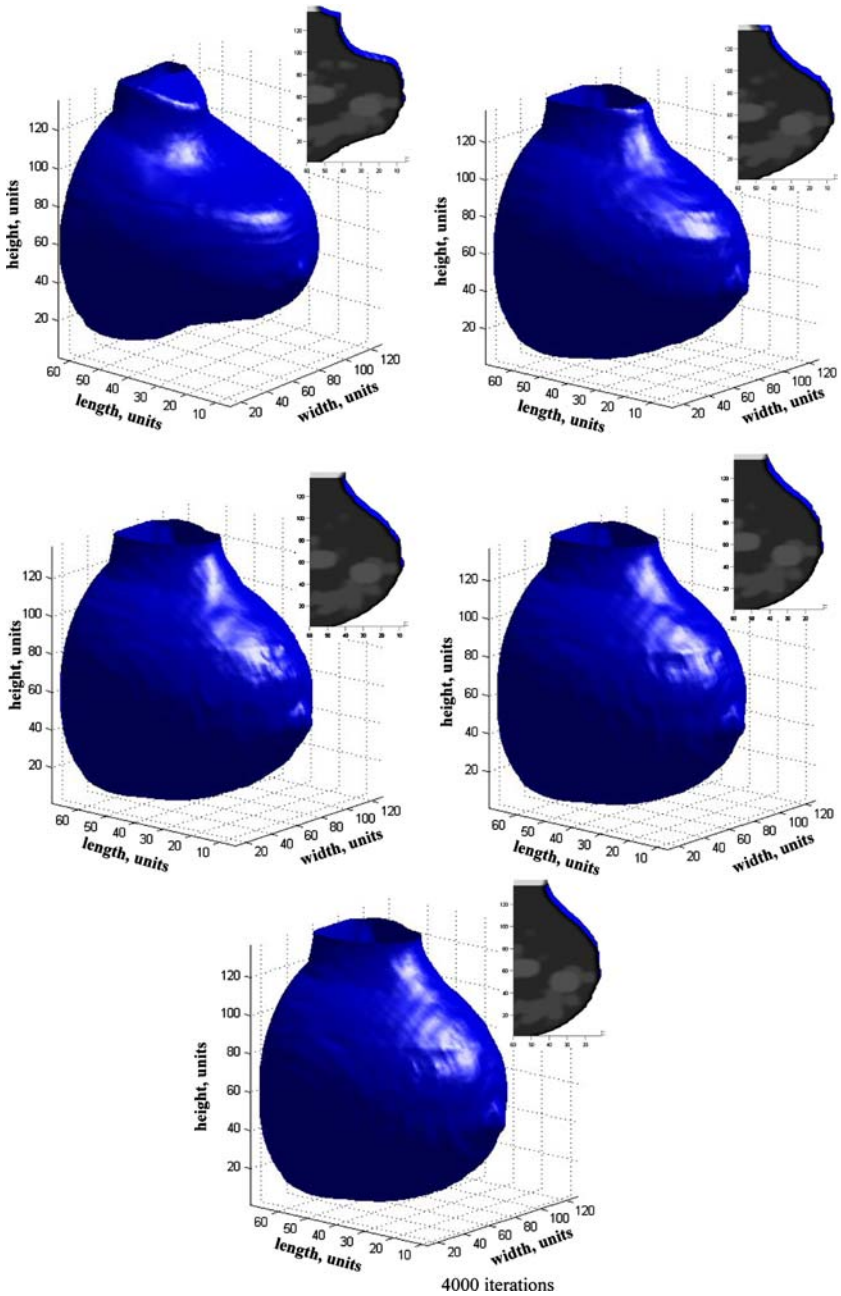

Fig. 11 3D views of the decompressed breast model after **a** 50, **b** 350, **c** 1,000, **d** 2,000 and **e** 4,000 iterations

In the case of breast compression, it was demonstrated that the algorithm could handle the generation of a high-resolution compressed breast phantom. Simulations of the compression process applied to the breast model showed that the shape of the breast as well as its internal geometry can vary significantly between its compressed and uncompressed state. The position of the tissues inside the breast change significantly during compression, which could lead in some cases to unsuccessful biopsy sampling. The visible evaluation of the slices in Fig. 8 shows that the compression process does not lead to significant deformation of the simulated breast abnormalities (Fig. 8a, b). They rather follow the expansion of the breast in the *xy* plane as expected and observed in the images shown in Fig. 8c, d. This was expected due to the higher stiffness of calcifications in comparison with the normal healthy breast tissue. Data for comparison are not provided because there are no available experimental studies that investigate the true displacements inside the breast during the compression process.

The comparison between the slices shown in Fig. 9a, b demonstrates that the model elements are shifted several units from their initial uncompressed positions (Fig. 9a). The total displacement of the breast edge is found to be

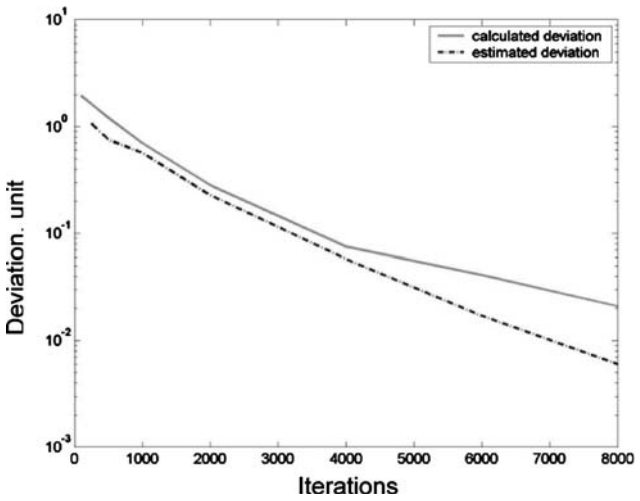

Fig. 12 Calculated and estimated deviation

more than 9 mm. Similarly, the comparison between uncompressed and compressed slices, shown in Fig. 9c, d, as well as those in Fig. 9g, h, shows that breast abnormalities are not subjected to a significant level of deformation. It can be concluded that the abnormalities maintain their shape and dimensions during compression, while the surrounding tissues (fat and gland) undergo considerable deformation and translation.

The average deviation (Fig. 10) of a random model element from its expected end position that would be calculated if the simulation lasts infinitely never exceeds 10% of the unit, which corresponds to less than 0.1 mm in the case under consideration. This means that if a node is shifted more than 10 units during compression, the corresponding deviation will be less than 1% of its whole displacement. Therefore, the accuracy can be considered to be adequate for simulation purposes. The computation time decreases significantly when the requirement for a high accuracy (ε) is diminished, leading to faster convergence.

The thickness of the compressed breast is rapidly regained in the process of reverse simulation. The breast regains its thickness in 1,000 iterations and restores completely its volume in more or less 4,000 iterations. The estimated deviation, presented in Fig. 12, does not vary significantly from the real deviation and the error is as close as 2% of the unit, when a convergence criterion of 10^{-4} units is settled as a requirement. These data provide verification for the reversibility of the compression method both by visual and numerical assessment.

The selected application of breast compression demonstrated the possibility of the SASTC to yield high-resolution compressed breast phantoms with a high accuracy, involving various tissues and structures and to perform an even higher resolution compression simulation. Simulation of breast compression in mammography using this algorithm could provide more realistic images that could serve for educational, clinical application and research purposes. The latter include investigations of different breast imaging techniques, involving compressed and uncompressed breasts.

5 Conclusions

This work presents a new general approach for modeling soft tissue compression process. The method, called SASTC, was successfully applied to compress a 3D breast model. Future work is directed to the introduction of nonlinear springs in the model, in order to come closer to the human tissue behavior, as well as the introduction of more complex boundary conditions (such as skin) in the breast under compression. A comparison of the proposed method with an FEM analysis is necessary to be accomplished as well. Future experimental work, using a hardware phantom, is also planned to provide experimental results for the purpose of this comparison.

References

1. Azar F, Metaxas D, Schnall M (2000) A finite element model of the breast for predicting mechanical deformations during biopsy procedures. In: Proceedings of the IEEE workshop on math methods in biomedical image analysis, pp 38–45
2. Azar F, Metaxas D, Schnall M (2001) A deformable finite element model of the breast for predicting mechanical deformations under external perturbations. Acad Radiol 8:965–975
3. Azar F, Metaxas D, Schnall M (2002) Methods for modeling and predicting mechanical deformations of the breast under external perturbations. Med Image Anal 6:1–27
4. Baumann R, Glauser D, Tappy D et al (1996) Force feedback for virtual reality based minimally invasive surgery simulator. Stud Health Technol Inform 29:564–579
5. Bliznakova K, Bliznakov Z, Bravou V et al (2003) A three-dimensional breast software phantom for mammography simulation. Phys Med Biol 48:3699–3719
6. Bliznakova K, Kolitsi Z, Pallikarakis N (2006) Dual-energy mammography: simulation studies. Phys Med Biol 51:4497–4515
7. Desbrun, Gascuel M (1995) Animating soft substances with implicit surfaces. In: Proceedings ACM SIGGRAPH
8. Luciani A, Jimenez S, Florens J et al (1991) Computational physics: a modeler simulator for animated physical objects. In: Proceedings of Eurographics conference, pp 425–437
9. Meseure P, Chailou C (1997) Deformable body simulation with adaptive subdivision and cuttings. In: Proceedings of the WSCG'97 conference,pp 361–370
10. Poulos A, McLean D (2004) The application of breast compression in mammography: a new perspective. Radiography 10:131–137
11. Wellman P, Howe R, Dalton E et al (1999) Breast tissue stiffness in compression is correlated to histological diagnosis. Technical report, Harvard Biorobotics Laboratory
12. Zienkiewich O (1977) The finite element method, 3rd edn. McGraw-Hill, New York